Le modèle en couches : vers une description unifiée de la structure nucléaire

A. Poves

LE MODÈLE EN COUCHES

(vers une description unifiée de la structure nucléaire) [1]

Alfredo Poves

Departamento de Física Teórica, Universidad Autónoma
Cantoblanco, 28049-Madrid (España)

RESUMÉ.
Nous présentons dans ce cours les fondements du modèle en couches sphérique, que l'on traite comme une approximation à la solution du problème séculaire complet. Nous introduisons les notions d'espace de valence, d'interaction effective et d'opérateur effectif. Nous analysons la structure des interactions effectives réalistes et nous associons la partie monopolaire de celles-ci avec le champ moyen sphérique. Le hamiltonien multipolaire est ramené à une forme universelle et simple contenant appariement (isoscalaire et isovectoriel), quadrupole, octupole, hexadecapole et $(\sigma \cdot \tau)$ $(\sigma \cdot \tau)$. Les méthodes de résolution du problème séculaire sont décrites, en particulier la méthode de Lanczos. Nous appliquons le modèle à la description de la déformation nucléaire et nous le mettons en rapport avec les théories du champs moyen déformé. Nous proposons une nouvelle symétrie, "quasi"-SU3, pour aborder la déformation en base sphérique. Finalement nous étudions les noyaux très éloignés de la vallée de stablité β en particulier en ce qui concerne la disparition de quelques unes des fermetures magiques que nous expliquons en termes d'états intrus.

ABSTRACT
In this series of lectures we present the foundations of the spherical shell model that we treat as an approximation to the exact solution of the full secular problem. We introduce the notions of valence space, effective interaction and effective operator. We analyse the structure of the realistic effective interactions, identifying their monopole part with the spherical mean field. The multipole hamiltonian is shown to have a universal (simple) form that includes pairing (isovector and isoscalar), quadrupole, octupole, hexadecapole and $(\sigma \cdot \tau)$ $(\sigma \cdot \tau)$. We describe the methods of resolution of the secular problem, in particular the Lanczos method. The model is applied to the description of nuclear deformation and its relationship with the deformed mean field theories is studied. We propose a new simmetry, "quasi"-SU3, to understand deformation in the spherical basis. Finally we discuss the domain of nuclei very far from the valley of β stability, adressing the vanishing of some magic closures that can be explained in terms of intruder states.

[1] Lectures given at the Ecole Internationale Joliot-Curie, "Structure nucleaire: Un nouvel horizon", September 1997.

SUMMARY

1.- **Introduction**

2.- **Basic notions of the Spherical Shell Model.**

The nucleus as a system of non-(explicitely)-relativistic nucleons. The nucleon-nucleon interaction. The independent particle model and the nuclear mean field. Regularizability of the nucleon-nucleon interaction in the nuclear medium. G-matrices and density dependence. The mean field as a basis for the occupation number space (Fock-space). Valence spaces; the secular problem. Examples of shell model valence spaces. The effective nuclear interaction written in second quantization formalism in jj coupling.

3.- **Realistic effective interactions.**

Monopole and multipole hamiltonians. The separation theorem. The monopole hamiltonian and the spherical mean field. Explicit expressions for the isoscalar and isovector monopole hamiltonian. What is right and what is wrong in the realistic effective interactions and how to cure it. An application; the quasi-particle gaps of ^{48}Ca and ^{56}Ni. Randomness and coherence in the multipole hamiltonian.

4.- **The solution of the secular problem.**

How to choose the basis; coupling schemes (m-scheme, JJ, quasi-spin, etc) and truncations. The Lanczos method. Whitehead's prescription for the calculation of strength functions. Shell Model Monte Carlo. Some spectroscopic results in the pf shell.

5.- **Spherical Shell Model and deformation.**

Rotors around A=48. Comparison of mean field and shell model results. Alignment and back-bending. A word on neutron-proton pairing. The limit of strong spin-orbit; Quasi-SU3 and Pseudo-SU3.

6.- **Nuclei far from stability.**

Magic numbers (Shell closures) far from stability; do they stand? The reduction of the shell gaps and the role of correlations. Intruder states. From ^{20}Mg to ^{40}Mg. N=20 and N=28 in very neutron rich isotopes. The N=Z line. The region of deformation around N=Z=40.

7 - **Conclusions.**

1. INTRODUCTION

The nuclear shell model has been often considered to be of application only to those nuclear manifestations in which the single particle degrees of freedom are dominant. That in spite of the work of Elliott [1], already 40 years old, that demonstrated the possibility of explaining deformation in light nuclei using the SU3 properties of the quadrupole nuclear force in an harmonic oscillator basis. In recent times the advent of new computers and shell model codes has given access to new mass regions where collectivity shows up in a more conspicous way, and the spherical shell model approach has proven to be able of coping with the new challenges, either close or far from the valley of stability, giving a unified description of the single particle and collective degrees of freedom of the nucleus. In this lectures we plan to guide the reader from the very basic starting points of the shell model description of nuclei to some of the latest applications. Our aim is to keep while possible the contact with the underlying free nucleon-nucleon interaction and when the link has to be broken to try to understand why. Many books exist that can serve as introduction to the subject, but we shall quote only the more recent or those that fully develop the mathematical formalism of the theory [2]. The last complete review of the shell model approach to nuclei is due to B. A. Brown and B. H. Wildenthal [3]

The original aspects of this presentation come from a long lasting collaboration with Etienne Caurier and Andres Zuker (Ires, Strasbourg), Joaquin Retamosa (UCM, Madrid), Frederic Nowacki (IPT, Strasbourg) and Gabriel Martinez-Pinedo (Caltech). Although adressed to a very different audience, there are two recent conference reports by A. Zuker that in some cases overlap and in others complement these notes [4].

2. BASIC NOTIONS OF THE SPHERICAL SHELL MODEL

We shall consider the nucleus as composed of Z protons and N neutrons, that interact via two-body forces and obey a non-relativistic (Schrödinger) equation. Therefore we will not consider explicitely meson or quark degrees of freedom nor shall we use relativistic kinematics. Recent advances in the relativistic mean field description of nuclei based on meson exchanges have shown that the main advantages of such an approach are that it accomodates the spin orbit interaction in a natural way, suggesting –perhaps– that its isospin dependence is different from what is assumed in the non-relativistic effective forces and that it provides a saturation mechanism for nuclear matter (see J. Mathiot's lectures in this volume). Many relativistic aspects are actually incorporated in the non relativistic approach via the nucleon-nucleon interaction in the vacuum that contains many terms of relativistic origin (spin-orbit, tensor etc). The problem of saturation can be solved in the non-relativistic approach by introducing three-body forces. In mean field effective interactions, density dependent terms take care of saturation. In the shell model approach the size of the underlying mean field potential is adapted to the size of the nucleus, although some problems originating in the regularization of the nucleon-nucleon interaction may show up in the spectroscopic calculations too.

The starting point is the nucleon-nucleon interaction V_{NN}. As it corresponds to a derived interaction it is not simple. It contains all kinds of terms, central, spin-orbit, tensor, spin-spin etc. At long distances it has a Yukawa form, while at short distances

it shows an extremely repulsive core. The short range repulsion is at the origin of most of the theoretical and technical problems that the nuclear many-body theories have to solve. Actually, the very idea of a shell model for the nucleus may seem contradictory with this strong correlation because it rudely breaks the independent particle picture. However, very early, experimental evidence of a shell model like behaviour was available – magic numbers, single particle energies, magnetic moments etc – that led to the empirical construction of the nuclear mean field, a surface corrected harmonic oscillator, whose main novelty was the very strong spin-orbit splitting needed to explain the experimental magic numbers.

$$V(r) = \frac{1}{2}m\omega^2 r^2 + Dl^2 + C\vec{l}\cdot\vec{s}$$

The success of the independent particle model implies that the bare nucleon-nucleon interaction can be regularized in the nuclear medium. Therefore an effective interaction can be found such that

$$H_{eff}\Psi_{eff} = H_{bare}\Psi_{correlated}$$

This effective interaction can be aimed to be used in mean field calculations along the periodic table and then it has to incorporate density dependent terms or for configuration mixing calculations, in this case its comes under the name of G-matrix. The main problem of the regularization procedures based on Brueckner theory is that they fail to reproduce the saturation point of nuclear matter (the Coester line problem). This is something to be recalled when using realistic G-matrices.

The use of a regularized interaction implies that what we are dealing with in a shell model description are quasiparticles in Landau's sense. This will show up in observables such as spectroscopic factors in (d,p) or $(e,e'p)$ reactions, Gamow-Teller strengths or partial shell occupancies as measured by electron scattering (the best know being the 3s1/2 orbit in lead isotopes). For a fully updated and accesible discussion of these points see ref [5] and J. P. Blaizot's lectures in this volume.

Once we adopt a regularized interaction that is compatible with the experimental mean field (magic numbers) we can proceed using the spherical mean field orbits as the basis for the occupation number space (Fock space). We have states i, j, k, ... with energies ϵ_i, ϵ_j, ϵ_k, ... that bunch in shells and give rise to magic numbers when the energy difference between them is large enough. The relevant operators create or anhilate a particle in a generic state "i" and second quantization formalism appears as the natural one.

A "formal" solution to the A-body problem can be sketched as follows:

i) We start by choosing a single particle basis, $a_i^+ \ |0>$,

ii) then, we build the A-particle wavefunctions,

$a_{i1}^+ \ldots a_{iA}^+ \ |0> = \mid \phi_\alpha >$

iii) in terms of which, the physical states are expressed as:

$\mid \Phi > = \sum_\alpha C_\alpha \mid \phi_\alpha >$

iv) The solution of the secular problem

$H \mid \Phi > = E \mid \Phi >$

v) is given by the eigenvalues and eigenvectors of the matrix

$< \phi_\alpha \mid \mathrm{H}_{eff} \mid \phi_{\alpha'} >$

What we call spherical shell model description is an approximation to this formal solution, using a finite number of many-particle states. The many-particle wavefunctions must have the quantum numbers associated to the symmetries of the Hamiltonian

$$\Psi(J,T)^\pi(N,Z)$$

The effective interaction H_{eff} can be written in jj coupling as:

$$\sum_i t_i + \sum_{ijkl} W^\Gamma_{ijkl}(a_i^+ a_j^+)^\Gamma (a_k a_l)^\Gamma$$

with Γ representing the pair J,T and $W^\Gamma_{ijkl} =< ij(JT)|V_{eff}|kl(JT) >$

The spherical mean field provides a basis and a zeroth order view of the nuclear dynamics. The regularized interaction is two-body and will govern the detailed behaviour of nuclei. For the mean field picture to have a sense, we expect that it will survive to the incorporation of the full interaction, at least in most of the cases, in other words, the separation between major shells will not collapse when the interaction is switched on. These constraints define the natural valence space (set of orbits) for a given class of nuclear properties. Let's be more precise on this point. For a given nucleus (N,Z) the mean field dictates which states are occupied (those below the Fermi level) and which are empty (those above). But other states can be close enough in energy or have such an structure that the residual two-body interaction can mix all of them and produce correlated states, deformed, superfluid or whatever. Therefore, the infinite set of mean field orbits will be divided in three parts:

a) **Inert core**, the orbits that are forced to be always full. Imagine that the core consists of $\mathrm{N_c}$ neutrons and $\mathrm{Z_c}$ protons, thus if we are studying a nucleus (N,Z) there will remain $\mathrm{n_v}$=N–$\mathrm{N_c}$ valence neutrons and $\mathrm{z_v}$=Z–$\mathrm{Z_c}$ valence protons.

b) **Valence space**, the orbits available to the valence particles, that will partially occupy them according to the dictates of the effective interaction.

c) **External space**, the remaining orbits that are always empty .

It is the task of the theory to find the valence spaces that contain the relevant degrees of freedom for a given problem as demanded by the effective interaction. In figure 1. we have sketched the spherical mean field at the stability valley for A$\leq$100. The safer valence spaces for shell model calculation are those comprised between magic closures. We shall examine several typical ones and see which properties they can accomodate and which not.

p-shell [1p3/2,1p1/2]. Calculations in this valence space can describe the behaviour of nuclei with 2<N,Z<8 (only positive/negative parity states in even/odd nuclei).

sd-shell [1d5/2,2s1/2,1d3/2]. Positive parity states of nuclei 8<N,Z<20.

pf-shell [1f7/2,2p3/2,2p1/2,1f5/2]. Although this valence space would naturaly cover nuclei with 20<N,Z<40, the strong spin orbit term of the spherical mean field breaks the harmonic oscillator ordering and beyond N,Z=32 the orbit 1g9/2 has to be explicitely included.

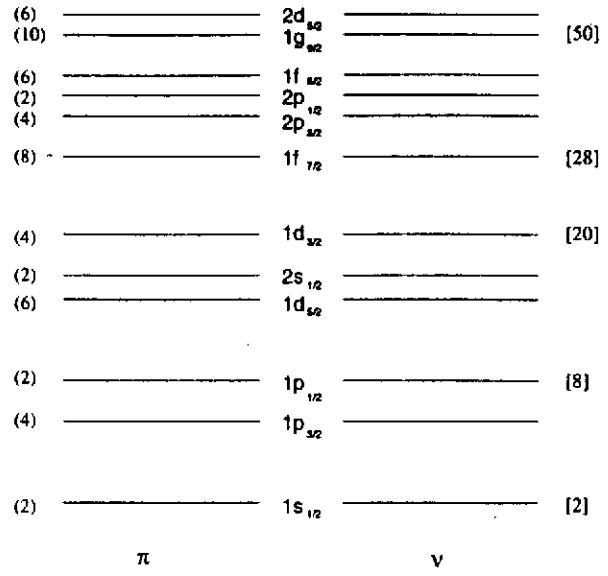

Figure 1: The spherical mean field close to the stability fo A$\leq$100

It is evident that doubly magic nuclei and their neighbours play a central role in this description. At the same time, in these valence spaces, they are represented by a single Slater determinant and if we were aiming to a description of their excited sates, another valence space containing orbits from two major shells had to be chosen. As an example, the first and second excited states of ^{16}O a 3^- (octupole vibration) and a 0^+ (head of a deformed rotational band) at around 6 MeV excitation energy can be described in the valence space [1p1/2,1d5/2,2s1/2] [6]. When the valence space allows for excitations into different major oscillator shells, one has to pay attention to the appearance of spurious states of the center of mass, kind of very disturbing guests that may destroy the calculation if not under full control.

Far from stability or for heavy nuclei, the proton and neutron valence spaces may have no common orbits. For instance for the very neutron rich (N>20) Al, Si, P, S, Cl, and Ar isotopes, a reasonable valence space is the sd-shell for the protons and the pf-shell for the neutrons.

The rapid increase in the size of the basis limits the number of orbits that can be active. Notice that for a number of valence particles n_v, z_v the number of different Slater deteminants that can be built in a given valence space goes as the product of the combinatorial numbers made with the degeneracy of the space and the number of active particles. This gives

$$\binom{6}{n_v}\cdot\binom{6}{z_v};\ \binom{12}{n_v}\cdot\binom{12}{z_v};\ \binom{20}{n_v}\cdot\binom{20}{z_v}$$

for the p, sd and pf shells respectively. Therefore there will always be properties excluded

from the description, as for instance negative parity states in an sd-shell calculation. Giant resonances would demand at least two contiguous major shells in the valence space which is not usually the case. Only spin-like giant resonances –magnetic dipole and Gamow-Teller– are naturally contained in $0\hbar\omega$ valence spaces. Clustering phenomena can be tagged in simple shell model calculations but again the full spatial correlation will demand huge valence spaces.

An example. We want to study the low energy spectrum of ^{12}C. We limit ourselves to positive parity states. The natural valence space is therefore the *p*-shell and we have an "alpha particle" core. The number of active particles is four protons and four neutrons. The two orbits of the *p*-shell are 1p3/2 and 1p1/2. The interaction is defined by the single particle energies of these two orbits in A=5, that we can extract from experiment, and 15 two body matrix elements $< ij(JT)|V_{eff}|kl(JT) >$, where ijkl may be any of the two orbits above. For instance if $i = j = k = l =$ 1p3/2, JT can take the values 01,10,21 and 30.

Let's focuss now in the 0^+ T=0 states of ^{12}C (these are the experimental quantum numbers of the ground state, but the same procedure holds for any other values of the total angular momentum and isospin). We can build such an state in five diffent ways corresponding to different particle distributions among the shells and different intermediate angular momentum and isospin couplings.

1.- $(1p3/2)^8$ (J=0,T=0) $(1p1/2)^0$ (J=0,T=0)

2.- $(1p3/2)^6$ (J=0,T=1) $(1p1/2)^2$ (J=0,T=1)

3.- $(1p3/2)^6$ (J=1,T=0) $(1p1/2)^2$ (J=1,T=0)

4.- $(1p3/2)^5$ (J=1/2,T=1/2) $(1p1/2)^3$ (J=1/2,T=1/2)

5.- $(1p3/2)^4$ (J=0,T=0) $(1p1/2)^4$ (J=0,T=0)

After that we compute the matrix of the Hamiltonian in this basis (better if you have a code to do all the angular momentum algebra cfp's etc), diagonalize and obtain eigenvalues and eigenvectors. Once this done for all the JT pairs you can draw the theoretical level scheme. With the wave functions you can compute the diagonal matrix elements of one body operators that give magnetic moments and quadrupole moments or the off diagonals whose squares represent the electromagnetic (or weak) reduced transition probabilities. Occupation numbers, spectroscopic factors and many other observables can also be obtained.

We have said nothing yet about the precise effective interaction to be used in the calculation. One way to proceed, that has been frequently used, is to determine empiricaly the two body matrix elements from a fit to selected energy levels (and in some, rare, cases also to transitions). For the *p*- shell this was done by Cohen and Kurath [7] while for the *sd*-shell there are different fits by Wildenthal [8]. Another is to try to keep as close as possible to realistic G-matrices. However, in this approach the empirical evidence is that some averages of matrix elements, actually those that associated to extensive operators as particle number or isospin are not well predicted in any G-matrix and have to be phenomenologically corrected. This kind of approach is dicussed in detail in [9] and will be the subject of the next section.

3. REALISTIC EFFECTIVE INTERACTIONS

In this section we shall follow closely the work of M. Dufour and A. Zuker [10]. Their starting point is the so called separation theorem that states:

The effective interaction can be split in two parts: $H = H_m(monopole) + H_M(multipole)$ *where* H_m *contains all the terms that are affected by spherical Hartree-Fock variation and that, by this fact, are responsible for global saturation properties and spherical single particle behaviour.*

It has been shown in [10] that the monopole hamiltonian can be written as:

$$H_m = H_{sp} + \sum \left[\frac{1}{(1+\delta_{rs})} a_{rs}\, n_r (n_s - \delta_{rs}) + \frac{1}{2} b_{rs} \left(T_r \cdot T_s - \frac{3n_r}{4} \delta_{rs} \right) \right].$$

H_{sp} is the single particle term generated by the core orbits, the a and b coefficients are defined in terms of the centroids

$$V_{rs}^{T} = \frac{\sum_J V_{rsrs}^{JT}[J]}{\sum_J [J]}$$

as: $a_{rs} = \frac{1}{4}(3V_{rs}^1 + V_{rs}^0)$, $b_{rs} = V_{rs}^1 - V_{rs}^0$, and the sums run over Pauli allowed values.

This Hamiltonian gives the full energy when applied to closed shells and closed shells plus or minus a particle. In other words it determines the evolution of the single particle fields inside the model space. As commented before it is at this point that the defaults of the realistic G-matrices –probably related to their bad saturation properties– show up. Lets develop an example in the pf-shell. Starting with the experimental single particle energies of ^{41}Ca and the G-matrix obtained by Kuo and Brown [11] it is possible to obtain the quasiparticle gap around ^{48}Ca and ^{56}Ni in terms of the single particle energies and the centroids defined above, using the expressions:

$$\Delta(^{48}Ca) = -2B_e(^{48}Ca) + B_e(^{49}Ca) + B_e(^{47}Ca) = \varepsilon_p - \varepsilon_f + 8V_{fp}^1 - 7V_{ff}^1.$$

$$\Delta(^{56}Ni) = -2B_e(^{56}Ni) + B_e(^{57}Ni) + B_e(^{55}Ni) = \varepsilon_p - \varepsilon_f + 16a_{fp} - 15a_{ff} + \frac{3}{4} b_{ff}.$$

The results for the KB interaction are:

$\Delta(^{48}Ca) = 2.06$ MeV and $\Delta(^{56}Ni) = 3.42$ MeV

while the experimental numbers are:

$\Delta(^{48}Ca) = 4.81$ MeV and $\Delta(^{56}Ni) = 6.39$ MeV

similar numbers are obtained for the other G-matrices available. All of them give too much attraction between filled and empty shells reducing dangerously the gaps and driving the calculations to collapse. A very spectacular consequence of this unphysical reduction of the gap is that in a full pf shell calculation for ^{56}Ni using KB, the ground state, instead of a closed shell is a 4-particles 4-holes state, with deformation $\beta = 0.3$, head of a rotational band.

In order to restore the correct physical picture, the T=1 centroids of the interaction between the 1f7/2 orbit and all the others have to be made more repulsive of about 300 keV. Once this done the agreement with the large body of experimental data becomes

excellent. As a conclusion, *a necessary condition for good shell model spectroscopy is to have a good spherical mean field.* We will see later that if realistic G-matrices are used, it is also sufficient.

The multipole Hamiltonian H_M is what is left of H when it has been made monopole free. We expect it to contain pairing plus quadrupole, plus surely other terms. But whose are they? and how many?, can we expect to unveil some hidden simplicity out of the shell model interactions, that usually appear as long strings of numbers?

Lets start writing H_M in two different ways:

$$H_M = \sum_{r\le s,t\le u,\Gamma} W^{\Gamma}_{rstu} Z^{+}_{rs\Gamma}\cdot Z_{tu\Gamma}, \quad \text{or}$$

$$H_M = \sum_{rstu\Gamma} [\gamma]^{1/2} \frac{(1+\delta_{rs})^{1/2}(1+\delta_{tu})^{1/2}}{4} \omega^{\gamma}_{rtsu}(S^{\gamma}_{rt}S^{\gamma}_{su})^0,$$

where Z^{+}_{Γ} is the coupled product of two creation operators and S^{γ} the coupled product of one creation and one anhilation operator (see [10] for their precise definition). The matrix elements are related through,

$$\omega^{\gamma}_{rtsu} = \sum_{\Gamma}(-)^{s+t-\gamma-\Gamma} \begin{Bmatrix} r & s & \Gamma \\ u & t & \gamma \end{Bmatrix} W^{\Gamma}_{rstu}[\Gamma],$$

$$W^{\Gamma}_{rstu} = \sum_{\gamma}(-)^{s+t-\gamma-\Gamma} \begin{Bmatrix} r & s & \Gamma \\ u & t & \gamma \end{Bmatrix} \omega^{\gamma}_{rtsu}[\gamma].$$

Replacing pairs by single indeces $rs \equiv x$, $tu \equiv y$, $rt \equiv a$ and $su \equiv b$ in the above equations, we bring the matrices W^{Γ}_{xy} and $f^{\gamma}_{ab} = \omega^{\gamma}_{ab}\sqrt{(1+\delta_{rs})(1+\delta_{tu})}/4$, to diagonal form through unitary transformations $U^{\Gamma}_{xk}, u^{\gamma}_{ak}$:

$$U^{-1}WU = E \Longrightarrow W^{\Gamma}_{xy} = \sum_{k} U^{\Gamma}_{xk}U^{\Gamma}_{yk}E^{\Gamma}_{k}$$

$$u^{-1}fu = e \Longrightarrow f^{\gamma}_{ab} = \sum_{k} u^{\gamma}_{ak}u^{\gamma}_{bk}e^{\gamma}_{k},$$

and then,

$$H_M = \sum_{k,\Gamma} E^{\Gamma}_{k} \sum_{x} U^{\Gamma}_{xk} Z^{+}_{x\Gamma}\cdot \sum_{y} U^{\Gamma}_{yk} Z_{y\Gamma},$$

$$H_M = \sum_{k,\gamma} e^{\gamma}_{k} \left(\sum_{a} u^{\gamma}_{ak} S^{\gamma}_{a} \sum_{b} u^{\gamma}_{bk} S^{\gamma}_{b}\right)^0 [\gamma]^{1/2},$$

which we call the E and e representations.

For the diagonalizations the KLS force [12] in two contiguous major shells was used because the matrix elements were easily generated, but no difference with other G-matrices is to be expected. For the E representation the density of eigenvalues is asymmetric with a long tail to the left, which is what to expect of an attractive force. For the e representation the result is shown in Fig. 2. When the contributions to H_M of the five largest peaks (in absolute value) are eliminated, the E histogram in Fig. 3 becames symmetric, the residual skewness being associated with the three isolated peaks. French and Mon [13] have shown that a symmetric E distribution is all that is needed to characterize a

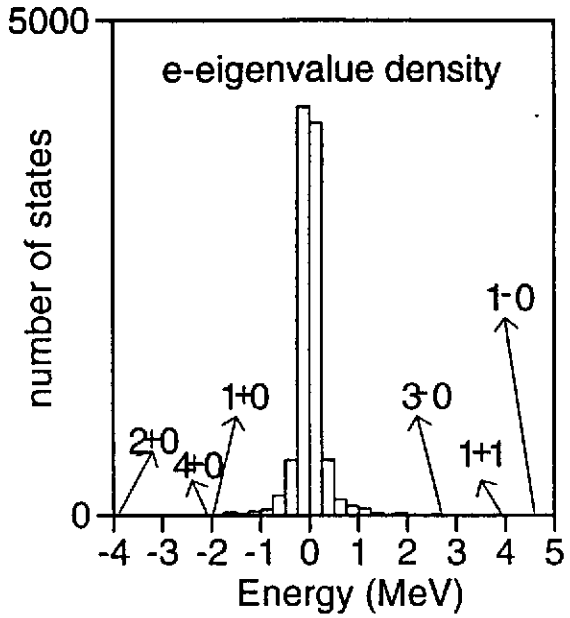

Figure 2: e-eigenvalue density for the KLS interaction in the pf+sdg major shells. The largest ones are shown by arrows.

random Hamiltonian. Therefore, we conclude that the five peaks extracted from the e distribution, plus the three big ones left in the E distribution design the candidates to a realistic collective Hamiltonian.

The rewarding aspect of this decomposition is that, not only the multipole hamiltonian can be reduced to a few terms, besides, these terms are simple (pairing is L=0 LS pairing, quadrupole is Elliott quadrupole γ =11 is $\sigma\tau \cdot \sigma\tau$ etc) and universal in a double sense; they are nearly equal for all different effective interactions and their mass dependence is well undestood.

4. THE SOLUTION OF THE SECULAR PROBLEM

In large scale shell model calculations the strategy to build and diagonalize the secular matrix is a major issue. First one has to decide in which coupling scheme to work. The simplest one is the so called $m - scheme$, whose basis is formed by all the Slater determinants contained in the valence space. It has the advantage of eliminating all Racah algebra, cfps, etc. The inconvenient is that the full dimension of the basis has to be carried on. The other choice is to implement "a priori" the symmetries of the Hamiltonian in the construction of the many particle basis. The full matrix is then divided in blocks and for each ensemble of values of the pertinent quantum numbers the dimensions are smaller. This approach is called "coupled scheme". The drawback is that the computational simplicity of the m-scheme gets lost. Usually only the exact quantum numbers JT are explicitely shown, however, approximate symmetries can be implemented, for instance seniority, that can make truncation procedures much more efficient.

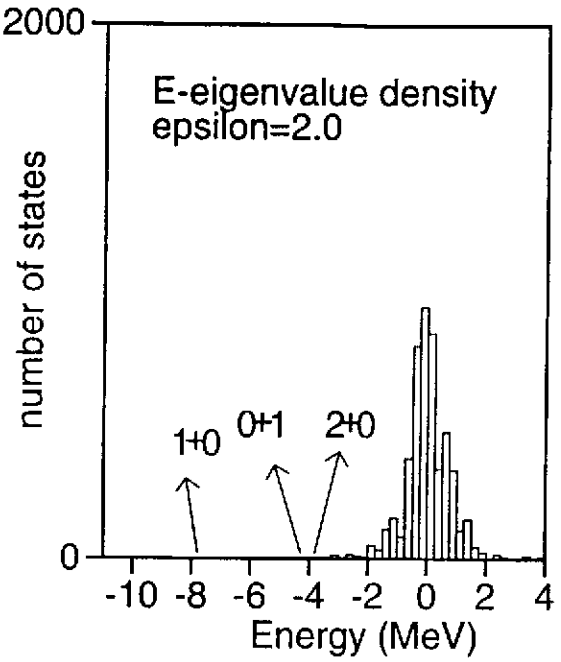

Figure 3: E-eigenvalue density for the KLS interaction in the pf+sdg major shells $\hbar\omega = 9$, after removal of the five largest multipole contributions. The largest ones are shown by arrows.

In order to obtain the relevant eigenvalues and eigenvectors two routes are available, either to build the full matrix and proceed by direct diagonalization or to use other methods as Lanczos' to obtain a part of the spectrum. For very large matrices the direct diagonalization approach is excluded due to computer size limitations, so we will concentrate in the Lanczos method. Let's mention however one of the first modern shell model codes, the Rochester Oak-Rigde MULTISHELL, a coupled, direct diagonalization code, based on the formalism of B. French [14]. Most of the present expertise in m-scheme Lanczos shell model codes has its roots in the Glasgow code made by Whitehead and collaborators [15].

In the Lanczos method the following iteration procedure is used:

- A starting vector ("pivot") is taken in the space. It can be chosen at random, be an approximation to the solution, a doorway etc. The choice of pivot influences the convergence properties of the procedure, but not the final results.

- Denoting the pivot as $|0>$ we construct $|1>= [\text{H-}<0|\text{H}|0>]|0>$ and normalize it to obtain $|\bar{1}>$. This is the second state of the Lanczos basis and we can already build a 2x2 matrix whose eigenvalues are approximations to the exact ones.

- We continue adding vectors to the basis

$\text{H}|\bar{1}>= \text{H}_{01}\ |0> + \text{H}_{11}|\bar{1}> + \text{H}_{21}|\bar{2}>$

- By construction at iteration N we have a tridiagonal N-dimensional matrix. The process has variational properties and the convergence for the lowest eigenvalues is very efficient.

Furthermore, the Lanczos method may be used to compute global properties of the spectra, even if approximate, via the calculation of strength distributions. The idea, due to Whitehead [16] is very simple. Suppose the ground state $|G>$ of a given nucleus has been obtained by the conventional Lanczos method. Let Ω^λ denote the multipole operator we are interested in. Acting with Ω^λ on $|G>$ we obtain the sum rule state (or the doorway). It is not a physical state if H do not commute with the multipole operator, but its norm is the sum rule or equivalently the total strength of the multipole operator in the ground state of the nucleus. Lets call its normalized version $|\Lambda>$ and develop it in energy eigenstates as:

$$|\Lambda>=\frac{1}{N}\sum_E S(E)|E>$$

where

$$N^2=\sum_E S^2(E)$$

and $S^2(E)$ is the strength function. The equality

$$<\Lambda|\mathrm{H^n}|\Lambda>=\frac{1}{\mathrm{N^2}}\sum_{\mathrm{E}}\mathrm{S^2(E)E^n}$$

shows that, taking $|\Lambda>$ as the pivot, each Lanzos iteration brings in the expectation value of two new powers of H on $|\Lambda>$, therefore after N iterations we have 2N moments of the strength function $S^2(E)$. Diagonalizing the Lanczos matrix after N iterations, the overlaps of the eigenvectors with $|\Lambda>$ give an approximation to $S^2(E)$ which has the same lowest 2N moments. In other words, one starts with a single peak that contains all the strength located at the centroid. Iteration after iteration it goes on fragmenting until the number of iterations equals the dimension of the basis. However, for a relatively small number of iterations we should have already a very good understanding of the global behaviour of the strength.

In figure 4. we give one example of this method in the case of the Gamow Teller strength function of ^{48}Ca. We went to 700 iterations (the number of 1^+ T=3 states in ^{48}Sc being 8590) and smoothed the peaks with gaussians of the experimental width to compare with the results of (p,n) experiments. Beyond the agreement and other matters, as the spreading of the experimental strength compared with the calculated one in the high energy region, due to the mixing with configurations outside the space, this is an illustration of the ability of the shell model approach to describe resonances in large valence spaces.

The problem of the size of the shell model spaces has motivated other –approximate– ways of solving the secular problem. The first one is the Shell Model Monte Carlo method, (see ref. [17] for a complete review) that treats the problem statistically introducing a partition function $e^{\beta H}$ where β is the inverse of the temperature. The problem involving two body propagation is amenable to a superposition of one body propagations by using the Hubbard-Stratonovich transformation. The multidimensional integrals are then evaluated by Monte Carlo sampling. The advantage of the method is that, as the problem remains essentially that of one body dynamics, the dimensions of the basis are tractable. However the method demands many different extrapolations; first in temperature (T→0), and then in some parameters added to the interaction in order to overcome the sign problem of the realistic interactions. It suffers also of limitations in the treatment of excited

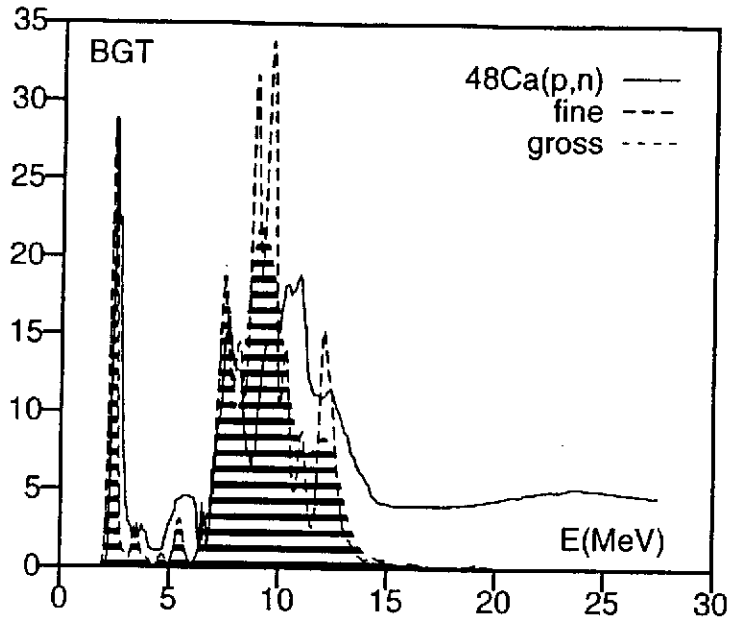

Figure 4: ^{48}Ca (p,n) ^{48}Sc cross section compared with the calculated Gamow Teller strength function using the Lanczos method

states because the cooling selects naturally the ground state. One final remark is that the method is very well suited to study finite temperature properties with the caveat, common to every shell model approach, that beyond some excitation energy the valence space will run out of states and the description will be unphysical.

Recently the same type of approach using the partition functions and Monte Carlo techniques has been applied in a quite different way in ref [18]. These techniques are used to sample the Hilbert space searching for an optimal, hopefully small, basis in which to diagonalize the full hamiltonian (Quantum Monte Carlo Diagonalization Method). The starting basis vectors are mean field solutions that break the symmetries, therefore projections have to be enforced and the method ressembles to the GCM used since long in other contexts.

Some spectroscopic results in the pf-shell

In the last years it has been possible to tackle the shell model description of nuclei in the pf shell using the $m-scheme$ code ANTOINE written by E. Caurier and a realistic effective interaction (KB3) obtained from the Kuo-Brown G-matrix [11] with the necessary monopole corrections [19] in line with what we have already discussed. The results are fully satisfactory and we shall only present here a couple of level schemes and a few tables that give an idea of the quality of the description. For a complete discussion of the pf shell see refs. [20, 21, 22, 23, 24].

In figures 5 and 6 the theoretical predictions are compared with the experimental results in the odd-odd nucleus ^{48}V and in the even-odd ^{49}V in both cases the agreement is excellent for the low spins and also for the high spin states. These are representative of the type of agreement obtained in all the cases studied

In tables 1,2 and 3 we have selected some electromagnetic and weak observables, mag-

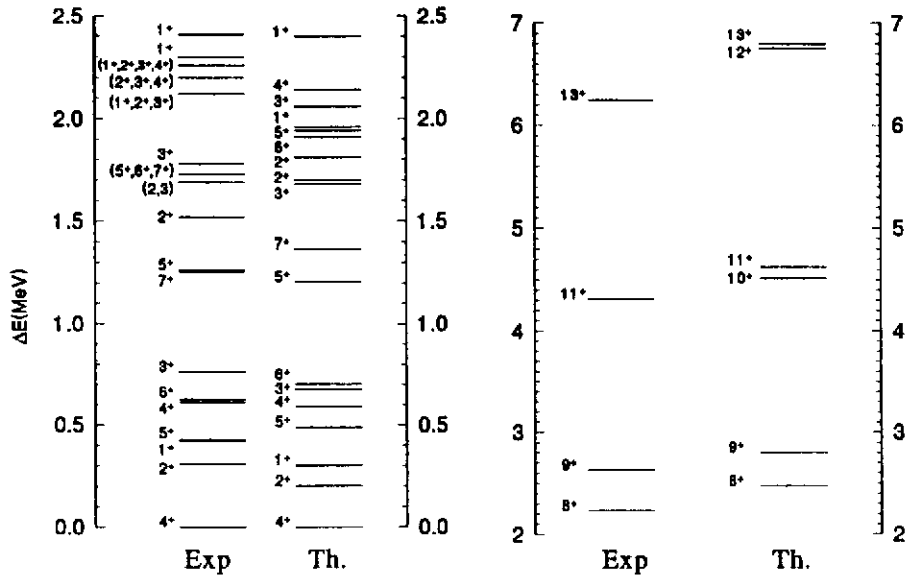

Figure 5: Energy levels of ^{48}V

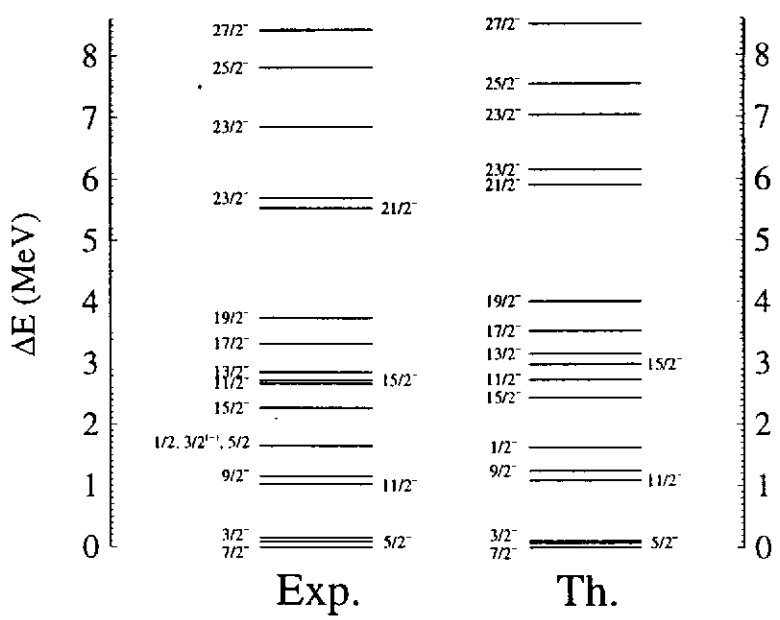

Figure 6: Energy levels of ^{49}V

Table 1: Dipole magnetic moments and quadrupole electric moments of the $A = 49$ isobars.

Nucleus	State	μ (μ_N)		Q (e fm^2)	
		Expt.	Theor.	Expt.	Theor.
^{49}Ca	$3/2^-$ (g.s.)	$-1.38(6)$	-1.46		-3.95
^{49}Sc	$7/2^-$ (g.s.)		5.38		-19.3
^{49}Ti	$7/2^-$ (g.s.)	$-1.10417(1)$	-1.12	24(1)	22
^{49}V	$7/2^-$ (g.s.)	$\pm 4.47(5)$	4.37		-11.1
	$3/2^-$ (0.153)	2.37(12)	2.25		18.87
^{49}Cr	$5/2^-$ (g.s.)	$\pm 0.476(3)$	-0.50		36.1
	$19/2^-$ (4.365)	7.4(12)	6.28		-3.43
^{49}Mn	$5/2^-$ (g.s.)		-3.24		36.4

Table 2: Experimental *vs* theoretical half-lives in the isobaric multiplets A=47 and A=49.

Nucleus	Half-Life		Fermi (%)	
	Expt.	Theor.	Expt.	Theor.
^{47}Ca	4.336(3) d	4.20 d		
^{47}Sc	3.3492(6) d	3.79 d		
^{47}V	36.6(3) m	20.7 m		
^{47}Cr	500(15) ms	480 ms	78.7	76.1
^{47}Mn		65.2 ms		54.1
^{47}Fe		18.7 ms		26
^{49}Ca	8.718(6) m	3.17 m		
^{49}Sc	57.2(2) m	41.4 m		
^{49}V	330(15) d	1088 d		
^{49}Cr	42.3(1) m	38.2 m		
^{49}Mn	382(7) ms	398 ms	72	75
^{49}Fe	75(10)	55 ms	61	42

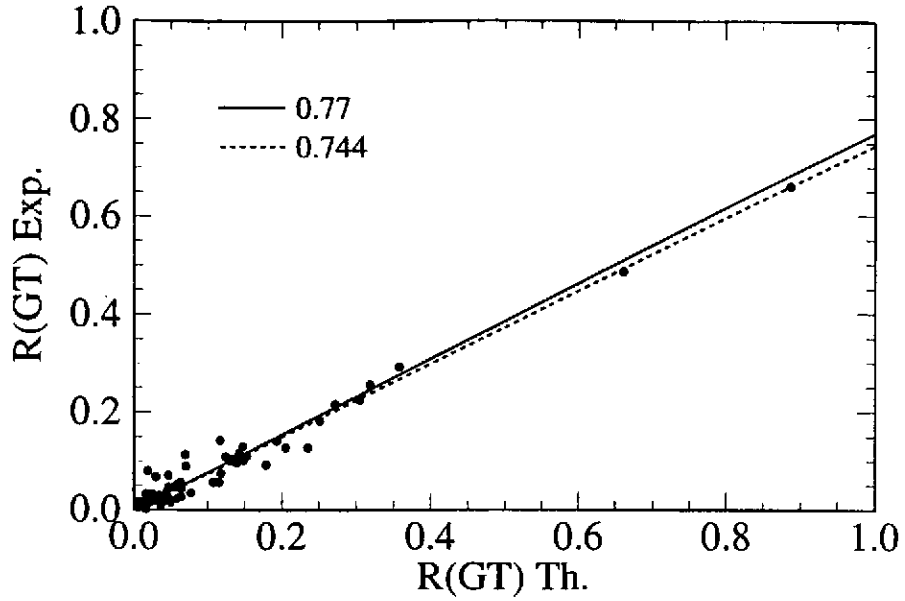

Figure 7: Individual Gamow-Teller reduced transition probabilities in the pf-shell, experiment *vs.* theory

netic and quadrupole moments and half-lives. In all cases the agreement with experiment is very good and we can safely make predictions for other cases in which there are no experimental measures.

Finally in figure 7 we have collected the Gamow-Teller matrix elements of many individual β decays for A=41 to 52. Comparing with experiment an effective value for the weak axial constant g_A(eff)=0.74 g_A(bare) is found. This result is consistent with the value extracted from similar comparisons in the p and sd shells and point to an asymptotic value of the renormalization of 0.7.

5. SPHERICAL SHELL MODEL AND DEFORMATION

We have seen how successful can be the shell model description of nuclei, provided a good valence space and a good effective interaction are used. We are therefore in solid grounds to address the topic of the collective behaviour in nuclei. We shall proceed to examine the following key questions:

- Can we describe rotational motion within the spherical shell model, beyond the *sd*-cases to which Elliott's SU3 is applicable?
- Which are the minimal valence spaces that contain the relevant degrees of freedom?
- Is there anything like an intrinsic state in the shell model wavefunctions?
- How compares the (spherical) shell model description whith the (deformed) mean field ones?

Some of these questions may sound rhetorical –and indeed they are!– but nonetheless their proper answers do not belong yet to the nuclear physics "common knowledge".

The pf-shell mass region could a very good place to study these aspects because full $0\hbar\omega$ calculations are still feasible and the mass and the number of active particles in the valence space make the link with heavy deformed nuclei much easier than in the very light cases. That, provided deformation shows up. But this is actually the case, as it is seen in figure 8 where the experimental level scheme of ^{48}Cr [25] is compared with the shell model calculation [26]. Notice the rotor-like spectrum up to J=10 and the backbending at J=12, reminiscent of the behaviour of heavier rotors. The E2 transition probabilities are fully collective and follow the Bohr-Mottelson prescription for a rotor in the strong coupling limit with a deformation β=0.3 (see table 3 for the experimental data [27]). Therefore, considering the nearly perfect agreement between experiment and theory in fig. 8 and in table 3, we can claim that ^{48}Cr is good candidate for a rotor amenable to a spherical shell model description. We want to be a bit more precise in our definition of a rotor and for that we shall rely in three indicators; i) the yrast band follows approximately a J(J+1) law, ii) the intrinsic quadrupole moment extracted from the B(E2) transition probabilities is constant for the different yrast states, ii) the intrinsic quadrupole moment extracted from the spectroscopic quadrupole moment is also constant for the yrast states and equal to the one extracted from the B(E2). The connexion between intrinsic and laboratory frame is made by the formulae [28]:

$$Q_0 = \frac{(J+1)\,(2J+3)}{3K^2 - J(J+1)}\, Q_{spec}(J), \quad \text{for } K \neq 1$$

$$B(E2, J \rightarrow J-2) = \frac{5}{16\pi}\, e^2 |\langle JK20|J-2, K\rangle|^2\, Q_0^2.$$

(for $K \neq \frac{1}{2}, 1$)

For even-even nuclei this is about as far as we can go in deciding whether we are faced with a good rotor or not. When a particle is added or removed, the collective model description of its coupling to the rotor leads to some very precise predictions that make the comparison with microscopic calculations more stringent in particular in what

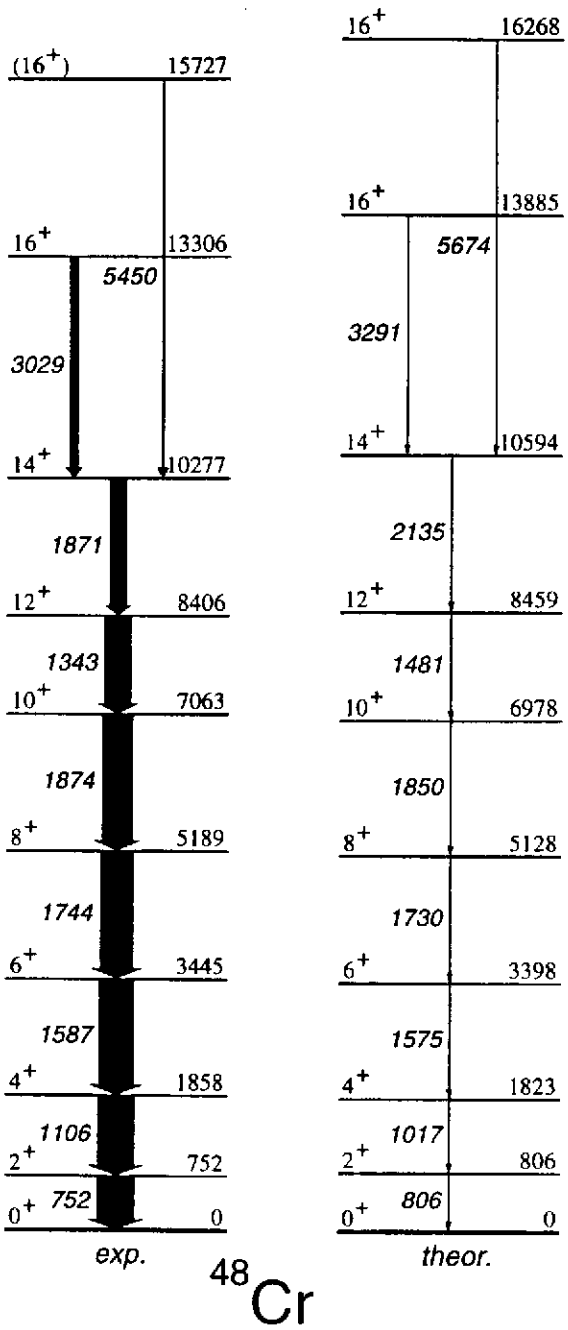

Figure 8: ^{48}Cr level scheme, experiment *vs.* theory

Table 3: Quadrupole properties of the yrast band of ^{48}Cr. B(E2) in e^2 fm^4, Q in e fm^2. The Q_0 values are extracted from the BE2's or the Q_{spec} as indicated

J	$B(E2)_{exp}$	$B(E2)_{th}$	$Q_0(B(E2))$	$Q_0(Q_{spec})$	Q_0[1f7/2, 2p3/2]
2	321(41)	228	107	103	104
4	330(100)	312	105	108	104
6	300(80)	311	100	99	103
8	220(60)	285	93	93	102
10	185(40)	201	77	52	98
12	170(25)	146	65	12	80
14	100(16)	115	55	13	50
16	37(6)	60	40	15	40

concerns magnetic properties. This analysis has been carried out in ref. [21] and we will not discuss it here.

Table 3 contains the information we were after, as given by the calculations (we use effective charges 1.5 for protons and 0.5 for neutrons). We have listed the B(E2) values, and the intrinsic quadrupole moments extracted from those, $Q_0(B(E2))$, or from the spectroscopic quadrupole moments, $Q_0(Q_{spec})$. The requirements stated above are fulfilled up to the backbending, therefore we can conclude that ^{48}Cr is a good rotor up to J=10 where the backbending takes place. The intrinsic quadrupole moment that we obtain corresponds to a deformation β=0.3 as we had anticipated. Notice that all the quadrupole properties of the full pf-shell calculation are reproduced (and even enhanced) if we reduce the valence space to the lowest two orbits, 1f7/2 and 2p3/2 (fp space). These results are shown in the last column of the table and give us the first hint on the minimal valence spaces that can accomodate deformed nuclei. The yrast band in the reduced space follows also the J(J+1) law although with a moment of inertia much larger than the experimental one.

Once the existence of a well behaved rotor is established, we can move around and ask ourselves what will happen if particles or holes are added to it. It has been shown in [21] that the mirror pairs ^{47}V-^{47}Cr and ^{49}Cr-^{49}Mn closely follow the semiclasical picture of a particle/hole strongly coupled to a rotor. When more particles or holes are added the collective behaviour starts disappearing, nevertheles even for ^{52}Fe (the largest detailed spectroscopic calculation ever made) a rotor like band appears at low spin and an yrast trap at $J=12^+$, both are accounted for in the shell model calculation [29]. Another exemple is ^{50}Cr that was predicted to be a double backbender in [30], prediction confirmed in a recent experiment [31] (see figure 9).

We have also the oportunity to compare the spherical shell model results with the deformed mean field ones, more precisely with the Cranked Hartree Fock Bogolyuvov calculations using the Gogny force [26]. The results for the yrast band are presented in figure 10. At first glance one could conclude that the CHFB model is doing a rather poor job in view of the discrepancies. However a closer look tell us that in fact all the experimental trends are there except for a too large moment of inertia. Due to that the CHFB E_γ's are systematically smaller than the experimental ones. But, from our discussion of the results in the reduced fp space, we are aware of the fact that the quadrupole properties may be right and the moment of inertia wrong. We know also that

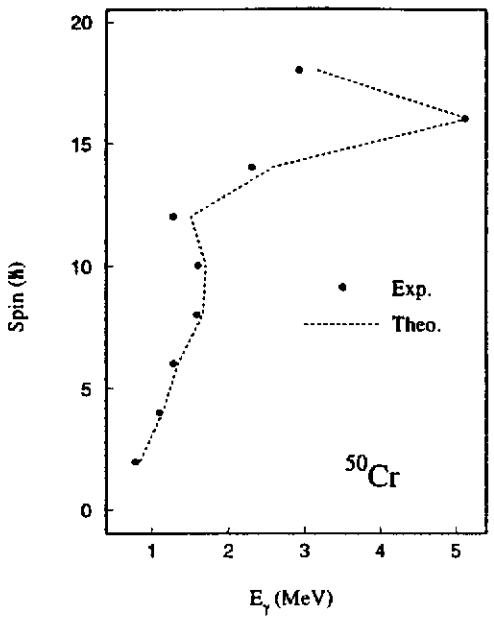

Figure 9: Backbending plot (J *vs* E_γ) of the yrast band of ^{50}Cr

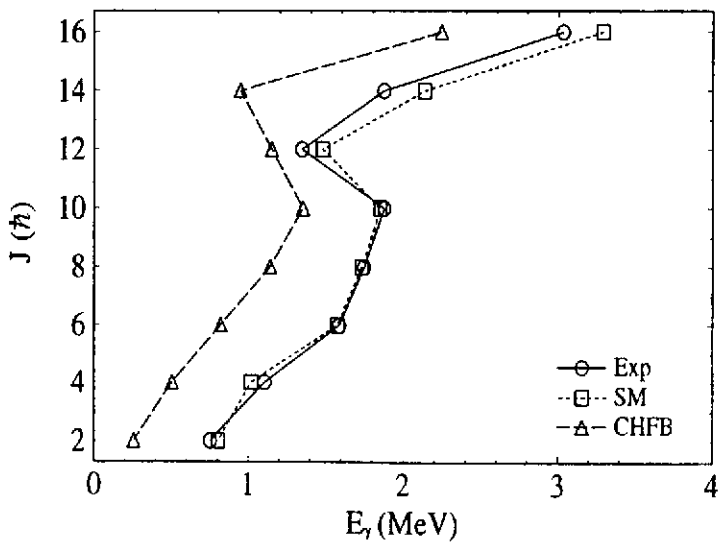

Figure 10: Backbending plot of the yrast band of ^{48}Cr. Shell Model (SM), Mean Field (CHFB) and experiment

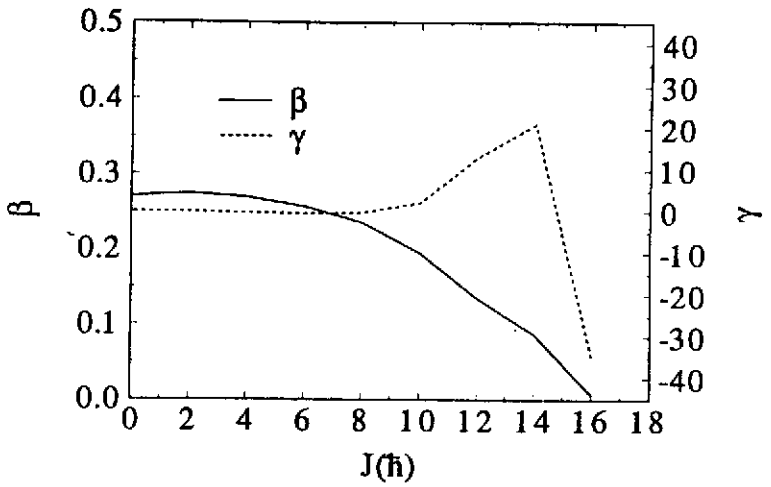

Figure 11: Deformation parameters β and γ as a function of J in the CHFB calculation

the decoupling of the quadrupole moment and the moment of inertia is a characteristic feature of the SU3 model of Elliott. So we go on with the comparison and in figure 11 we show the CHFB results for the intrinsic deformation parameters β and γ. We see that up to the backbending the nucleus is axially deformed with a deformation close to 0.3 that decreases slowly with J (0.2 at J=10) in full agreement with the shell model results. Beyond the backbending the deformation continues to decrease and there are some excursions into triaxiallity that are difficult to recast in collective terms. A very nice feature of the CHFB calculation is that it makes it possible to separate the contributions to the quadrupole moment coming from the core and from the valence orbits. The result, independent of J, is that both blocks contribute evenly, which is consistent with the effective charges we use in the shell model calculation.

In figure 12 we compare the fractional occupancies of the valence orbits in the two approaches. The similarities are striking and confirm the closeness of the wave functions obtained in the different descriptions. We learn from the figure that in the zone of the yrast band where the rigid rotor picture holds, the occupancy of the 2p3/2 orbit is large and constant. At the backbending, the decrease in deformation is correlated with its decrease in occupation. Here again we have an indication of the role of the fp orbits in the onset and offset of deformation. Actually, at high spin the configurations with p particles are geometrically hindered and the quadrupole correlations cannot develop. Another subtle difference is that the occupancy of the 1f5/2 orbit in the SM results is larger that in the CHFB ones, indicating a stronger pairing mixing.

Pairing *vs* quadrupole has been one of the classical themes in nuclear physics for ages. The advent of high spin physics and improven spectroscopic data in heavy N≈Z nuclei has brought up again an old question; how does pairing evolve with angular momentum? and then a new one; which is the role of proton neutron pairing close to N=Z? We shall examine these issues in what follows. To start with we select as our pairing T=0 and T=1 hamiltonians those extracted in ref. [10] from the realistic G-matrices (in this

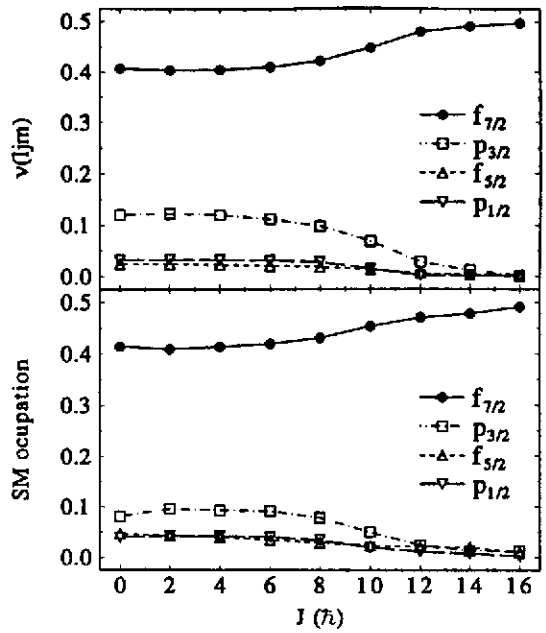

Figure 12: Fractional occupancies of the valence orbits in CHFB (upper panel) and SM (lower panel)

reference the analytical expressions –eq. 2.6– and the numeric values of the two body matrix elements –table I– can be found). We keep their notation and call P^{01} and P^{10} the isovector and isoscalar L=0 pairing hamiltonians. In order to evaluate the effect of pairing, we substract each pairing hamiltonian from KB3, make the calculations again and compare the results with the original ones.

The first, aparently unexpected, result is that for the states below the backbending – i.e. for those that can be viewed as proceeding of the same intrinsic, well deformed state– the wave functions with or without pairing have the same structure. To be more precise, their B(E2)'s and quadrupole moments are equal within a few percent and their overlaps are always better than 95%. This means that pairing does not affect the quadrupole properties that have somehow reached saturation in the deformed regime. This strongly suggest that:

- The differences between the CHFB and the SM results must be due to the deficiencies in the treatement of pairing in the mean field description.
- A calculation in the minimal valence space fp that reproduce the quadrupole properties can recover the correct moment of inertia including pairing in first order perturbation theory.

Having a look at figure 13, we realize that although the T=1 contribution almost doubles the T=0 one at J=0, it decreases more rapidly with increasing J, and already at J=6 they become comparable. At J=8 both reach a plateau and drop abruptly to zero at the band termination. Consequently T=0 pairing has to be properly taken into account when approaching N=Z. The same for the neutron proton part of T=1 pairing that amounts to one fourth of the total. To include them is not a very difficult task in the deformed regime, because, as we have just shown, perturbation theory will hold.

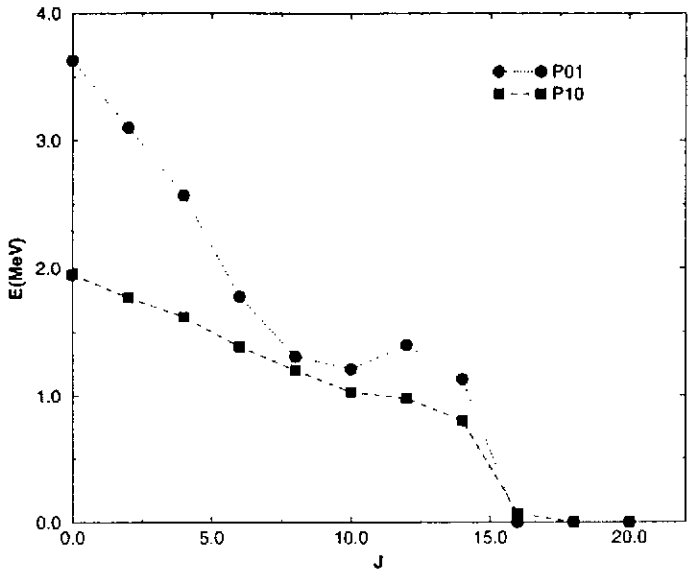

Figure 13: Isovector and isoscalar pairing contributions to the energy of the yrast states of ^{48}Cr

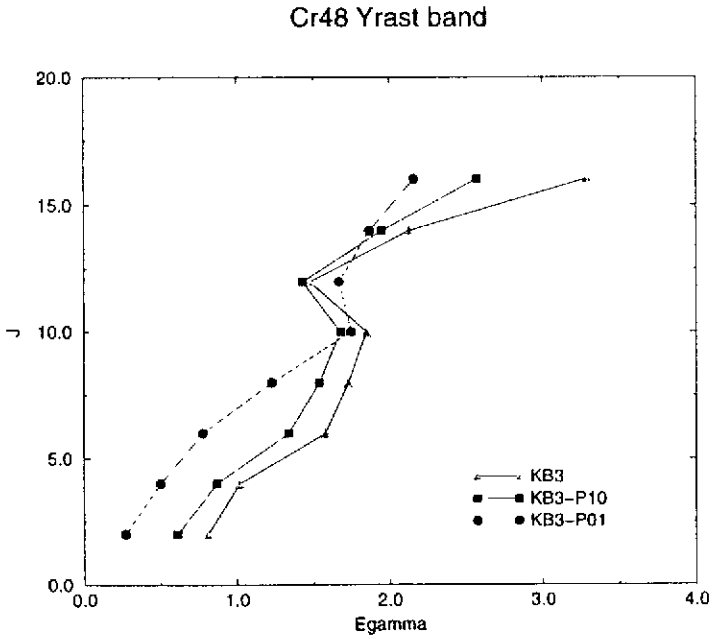

Figure 14: The effect of the isovector and the isoscalar pairing in the E_γ's along the yrast line in ^{48}Cr

We can now move to fig 14 where we compare the KB3 results with the results without T=0 and without T=1 pairing, in a backbending plot. Remember that the KB3 results and the experimental data are nearly indistinguishable. The efect of T=0 pairing is to make a paralel displacement of the KB3 line; the backbending stays at the same J, whereas the static moment of inertia is increased from the KB3 value 7.5 MeV^{-1} to 10 MeV^{-1}. Althoug the distorsion of the E_γ plot above the backbending is stronger if we take out the T=1 pairing, the same conclusions apply; backbending J unchanged, paralel displacement and increase of the moment of inertia to 20 MeV^{-1}. In view of these figures we can conclude that the difference in moment of inertia between the CHFB and the experiment is mostly due to the absence of neutron proton pairing in the Bogolyuvov description.

The indications coming from the study of these deformed nuclei have been used in [32] to investigate the symmetries underlying the development of rotational motion in nuclei. As we mentioned at the begining, the SU3 model of Elliott gives a laboratory frame description of nuclear deformation that is exact if the spherical mean field is the harmonic oscillator without spin-orbit splitting and the two body interaction has a quadrupole-quadrupole form. In this case SU3 commutes with the hamiltonian and rotational bands appear that can be traced back algebraically to an intrinsic deformed state. Everything we whished!!

Lets consider the quadrupole force alone, taken to act in the p-th oscillator shell. It will tend to maximize the quadrupole moment, which means filling the lowest orbits obtained by diagonalizing the operator $Q_0 = 2z^2 - x^2 - y^2$. Using the cartesian representation, $Q_0 = 2n_z - n_x - n_y$, we find eigenvalues $2p$, $2p-3$,..., etc., as shown in the left panel of Fig. 15, where spin has been included. By filling the orbits orderly we obtain the intrinsic states for the lowest SU(3) representations: $(\lambda, 0)$ if all states are occupied up to a given level and (λ, μ) otherwise. For instance: putting two neutrons and two protons in the $K = 1/2$ level leads to the ($4p$,0) representation. For four neutrons and four protons, the filling is not complete and we have the (triaxial) ($8(p-1)$,4) representation for which we expect a low lying γ band.

Next consider the influence of the spin-orbit splittting that will separate the subshells into two $\Delta j = 2$ groups. For even p we have the sequences $j = p + 1/2 \ldots 1/2$ below and $j = 3/2 \ldots p - 1/2$ above, while for odd p we have the sequences $j = p + 1/2 \ldots 3/2$ below and $j = 1/2 \ldots p - 1/2$ above. Let us keep only the lowest sequence and diagonalize again the quadrupole operator Q_0. We can keep only $\Delta j = 2$ sequences, because the $\Delta j = 1$ matrix elements are strongly suppressed both for large and small m, i.e., which lead to the orbits with largest oblate and prolate deformations respectively. The $\Delta j = 2$ matrix elements are practically identical to those in LS scheme if we make the identifications

$$l \longrightarrow j = l + 1/2 \quad m \longrightarrow m + 1/2 \times \mathrm{sign}(m).$$

The correspondence is one-to-one and the resulting "quasi SU(3)" quadrupole operator respects SU(3) relationships, *except* for $m = 0$, where the correspondence breaks down. Still, it suggests that sequences $j = 1/2,\ 5/2,\ 9/2 \ldots$ or $3/2,\ 7/2,\ 11/2 \ldots$, must have a behaviour close to that of the sequences $l = 0,\ 2,\ 4 \ldots$ or $1,\ 3,\ 5 \ldots$ that span the one particle representations of SU(3). The resulting spectrum for quasi-Q_0 is shown in the right panel of fig. 15. The result is not exact for the $K = 1/2$ orbits but a very good approximation.

The way to use the approximate quasi-SU(3) symmetry is simply to reason with the right panel of fig. 15 as we would do with the left one. Then, both the four and eight particle "representations" for $T = 0$ will be axial, while the ten particle $T = 1$ ones

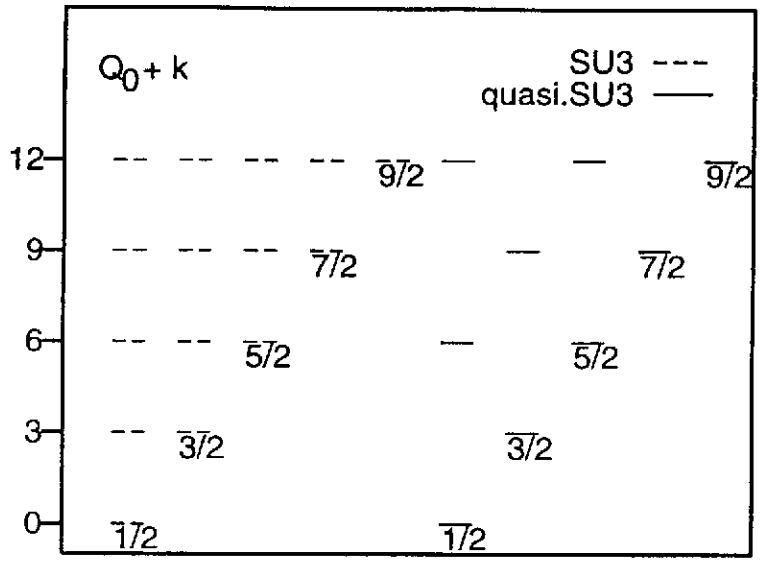

Figure 15: Nilsson orbits for SU(3) ($k = 2p$) and quasi-SU(3) ($k = 2p - 1/2$).

would be triaxial. At this point we note a positive indication in the absence of a γ band in ^{48}Cr (its counterpart in the *sd* shell, ^{24}Mg, is triaxial). It is then seen that the two lowest $\Delta j = 2$ sequence of orbits, separated from the rest by the spin-orbit splitting, are sufficient to ensure quadrupole coherence.

In most of the cases, when deformation sets in, these $\Delta j = 2$ groups are available, for instance, $(1d5/2, 2s1/2)^4$ gives deformation in ^{20}Ne, $(1d5/2, 2s1/2)^{4\pi}$ $(1f7/2, 2p3/2)^{2\nu}$ is the configuration dominant in the ground state of ^{32}Mg, $(1f7/2, 2p3/2)^8$ in ^{48}Cr, $(1g9/2, 2d5/2, 3s1/2)^8$ in ^{80}Zr etc. In the region of ^{80}Zr and beyond we can put this in correspondence with the Nilsson deformed mean field, that states that when nuclei acquire a stable deformation, two orbits K=1/2 and K=3/2 become occupied and rephrase it in spherical terms saying that rotational motion sets in when four protons and four neutrons are promoted to $\Delta j = 2$ blocks above the orbits normally filled. The normally filled orbits from which the particles are promoted turn out to form a Pseudo-SU3 sequence which reinforces the collectivity driven by Quasi-SU3. We have applied this extremely simple analytical model to the onset of deformation in the Nd, Sm, Gd and Dy getting B(E2) values in complete agreement with experiment without any extra parameter [32]. These QSU3-PSU3 combinations may be used to identify the spherical configurations responsible for superdeformation.

6. SHELL MODEL AND NUCLEI FAR FROM STABILITY

We have explained in detail that the two basic ingredients of the shell model description of nuclear dynamics are the effective interaction and the valence space. Furthermore, we have been able to get a better handle in the effective interaction by splitting it in the monopole and the multipole part. Which are the novelties to be expected when we try to describe nuclei far from stability? Let's avoid for the moment the very edge of the nuclear stability at the neutron rich side, the neutron drip line. For the other cases we use the same tools that we have developped close to the stability; first we determine the spherical mean field, that gives us the neccessary hints on the choice of the valence space and then we plug in the realistic multipole hamiltonian and solve the secular problem. From the earlier discussion it must be clear that it is the first requirement which is problematic. Because as we have mentioned repeatedly, the monopole part of the realistic interactions is unrealiable already at the stability. What make things worse in that the crucial data that are needed in order to fix the evolution of the spherical mean field are not yet available far from stability. This is the new challenge, to learn how the monopole hamiltonian evolves when the isospin has values that are much larger or much smaller than the values defining the line of β-stability. In order to reach this goal theory and experiment are bound to advance together.

There are already evidences of abnormal behaviour in the very neutron rich or very proton rich regimes that we can gather with the headline "vanishing of shell closures far from stability". It is however true that the cases presently known correspond only to semimagic nuclei. Let's start with the heavier example ^{80}Zr. It is a proton rich N=Z=40 nucleus. Z=40 is a solid shell closure in the doubly magic ^{90}Zr, however ^{80}Zr turns out to be an strongly deformed nucleus. For that to happen, the harmonic oscillator shell closure 40 has to be completely broken. Actually, the experimental results can be very well undestood if the yrast states of ^{80}Zr are given by configurations with eight holes in the pf-shell and eight particles in the sdg-shell. These configurations build a Pseudo-SU3 block in the hole orbits and a Quasi-SU3 block in the particle orbits that maximize the quadrupole moment and the quadrupole correlation energy. The gain in correlation energy of this 8p-8h configuration relative to the harmonic oscillator closed shell is about 25 MeV, the loss of monopole energy is more difficult to evaluate, however the experiment tells us is that it is less than 25 MeV. The mechanism comes up in all its simplicity; the monopole field locate different configurations at different unperturbed energies and each configurations has its own correlation energy. The balance of both energy contributions determines which configuration will be lower and in particular whether a shell closure will stand or vanish.

Long chains of isotopes from Ne to Ar are presently under experimental investigation. They give us the unique opportunity of exploring the behaviour of several magic closures in one single isotopic chain. We can also attempt to give a common description of the nuclei which show magic features and those in which the magicity disappears. We begin with the sulphur chain in which isotopes are known to be bound with N=10 up to N=32. In this case we come close to crossing three magic neutron numbers. The natural valence space for the protons is the sd-shell; for neutron number N$\leq$20 the sd-shell is also the right valence space, whereas beyond, either the pf-shell alone or both sd and pf will be needed. In the calculations of ref [33] we showed that the first choice is good enough, except in a small area around ^{31}Na. These calculations employed effective interactions for

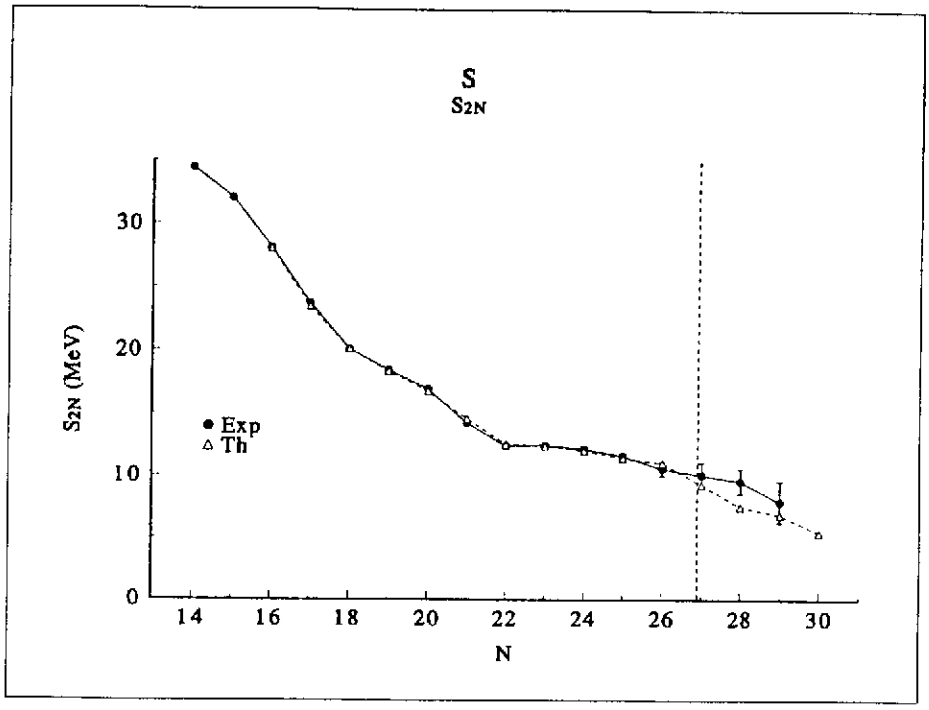

Figure 16: S_{2N} for the isotopes of sulphur

the two major shells that had been already tested in full $0\hbar\omega$ spaces, therefore describing in a consistent way isotopic chains that cover two major shells.

We show in figure 16 the comparison of the theoretical two neutron separation energies (S_{2N}) with the experimental results. Beyond the vertical line the experimental points are actually the extrapolated values from [34]. We see that the agreement is very satisfactory and do not deteriorates by crossing N=20, that appears to be a good closure for this isotope. At N=28 the discrepancy with the values from the systematics increases, which can bear a relation with the issue of the vanishing of the N=28 magic closure in the sulphur chain. This point was arisen by the mean field calculations of ref [35] that predicted deformation and shape coexistence in the sulphur isotopes around N=28. We discussed that in [33], arguing that the situation is better explained considering N=28 as a strongly correlated closed shell, than by the much stronger statement of no shell closure at all. The reasons are the following; the leading neutron configuration in the ground state of ^{44}S (that amount to 50% of the wave function) is $(1f7/2)^8$; the average occupancy of the 1f7/2 orbit is 6.95 compared to the maximum value 8.0; the excitation energy of the 2^+ increases relative to N=26 and N=30 (see fig. 17) and the BE2 slightly decreases compared to N=26,30. Therefore, even if strong correlations are present we do not think the N=28 shell closure has disappeared. Our calculated values agree with the results of recent experiments at MSU [36, 37] and GANIL [38].

The situation for Z$\geq$13 can be summarized as follows; N=20 stands as a neat shell closure (see [39] for an experimental reference on ^{34}Si); at N=28 the shell closure is eroded by the correlations and collective aspects show up in some cases, but this do not imply the vanishing of N=28 as shell closure.

Things change radically when we move to the neutron rich isotopes of neon, sodium and magnesium with N$\approx$20. It was pointed out many years ago that data on masses and

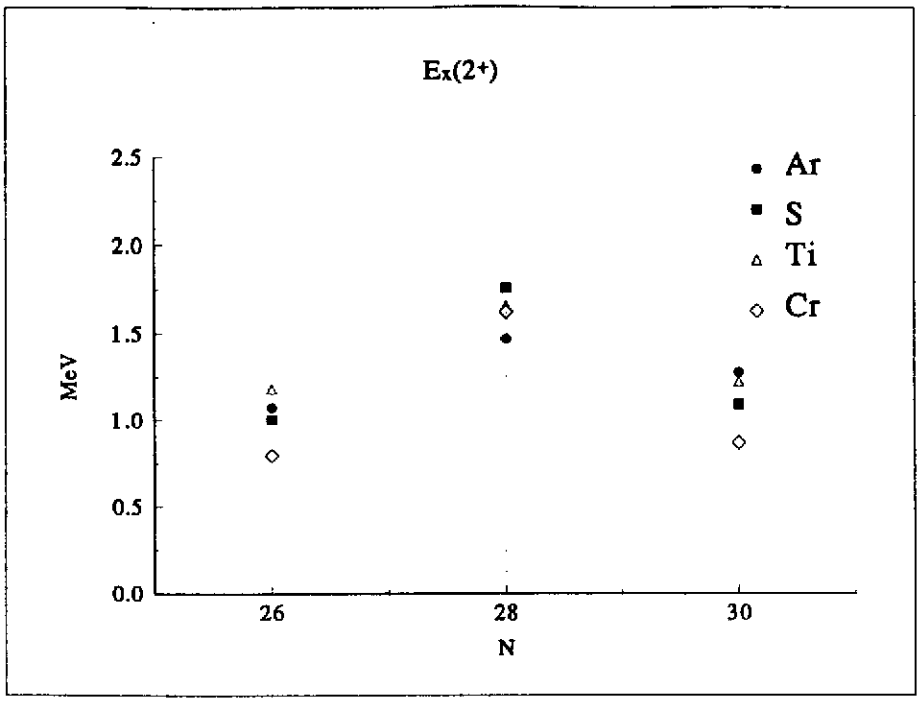

Figure 17: Excitation energy of the 2^+ states for several isotopic chains around N=28

ground state spins were incompatible with the persistence of the N=20 closure [40, 41]. Subsequent spectroscopic studies confirmed this hypothesis in particular because of the very low 2^+ in ^{32}Mg [42], the long lifetimes of several isotopes and the very high density of levels at very low energy in ^{31}Mg [43], in complete contradiction with the calculations that assumed N=20 to be closed [44]. Early theoretical explanations were given using a deformed mean field approach [45]. Later on a shell model interpretation in terms of deformed intruders was proposed [46] that has been confirmed by other shell model calculations [47, 48]. A very recent coulex experiment on ^{32}Mg [49] has measured a very large B(E2) $0^+ \rightarrow 2^+$ corresponding to β=0.5, in agreement with the theoretical predictions.

We have used the same effective interaction of [33] to push the shell model description to its limits, in order to settle the structure of these abnormal nuclei. We shall specialise our examples in the magnesium isotopes although we have results for all the nuclei in the region [50],

In figure 18 we compare the experimental S_{2N} with the predictions assuming N=20 closed. The agreement with the data is excelent for the Al isotopes, comparable to what we had found for larger Z's, but a clear discrepancy occurs at N=20 for the lighter elements. The discrepancy amounts to saying that N=20 is not bound enough. This was related to the breaking of the N=20 magicity.

The physics behind the vanishing of the N=20 shell closure far from stability is related to our discussion of the onset of deformation in section 5 and to our discussion on ^{80}Zr at the beginning of this section. The closed shell is protected by its gap, i.e. the energy the system looses if particles are promoted above it. But it is also vulnerable, because the configurations reached by opening the closed shell have, in general, a much larger correlation energy. The final result depends solely on the local behaviour of the effec-

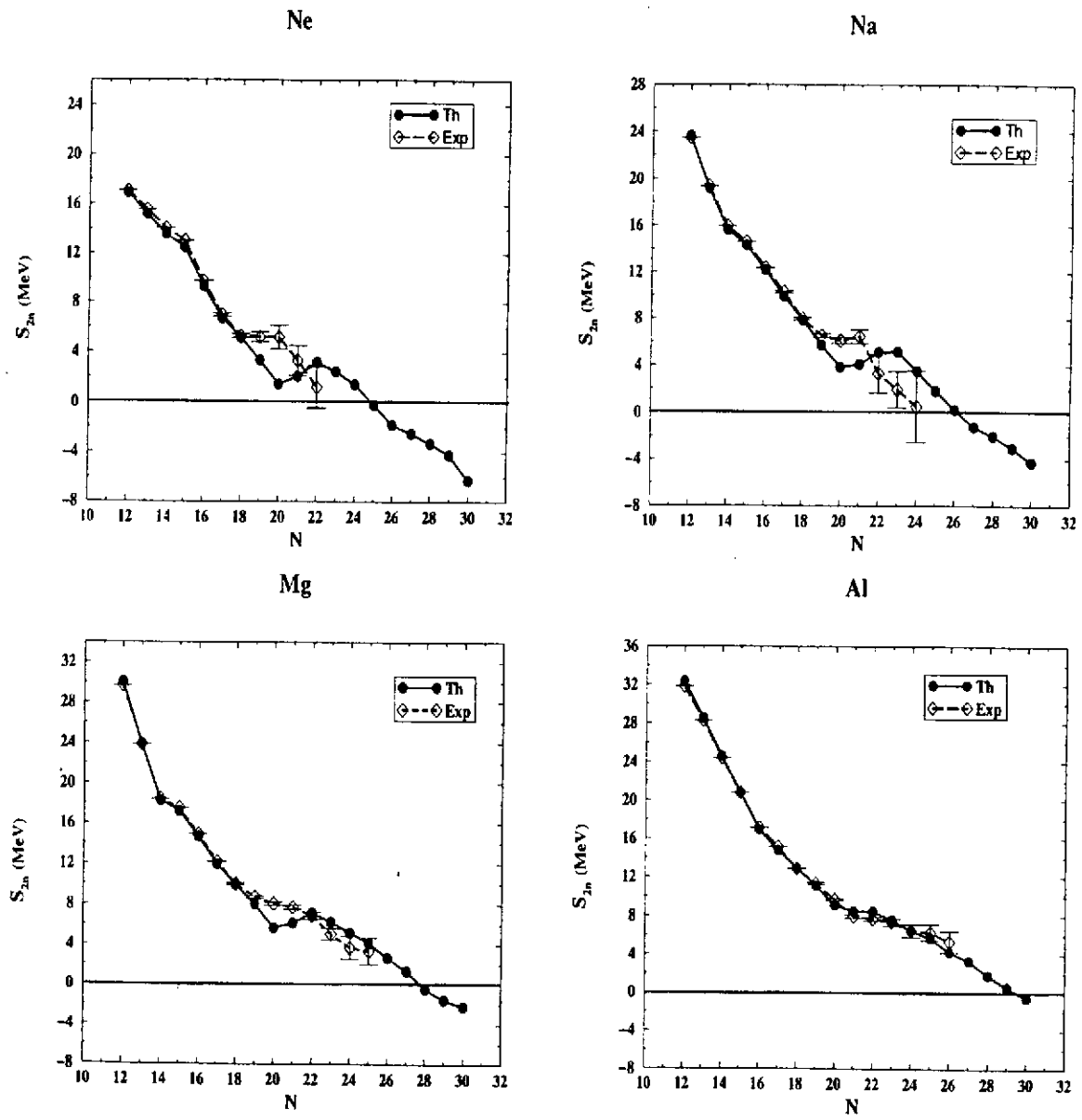

Figure 18: Two neutron separation energies, th. *vs* exp. , Ne, Na, Mg and Al isotopes

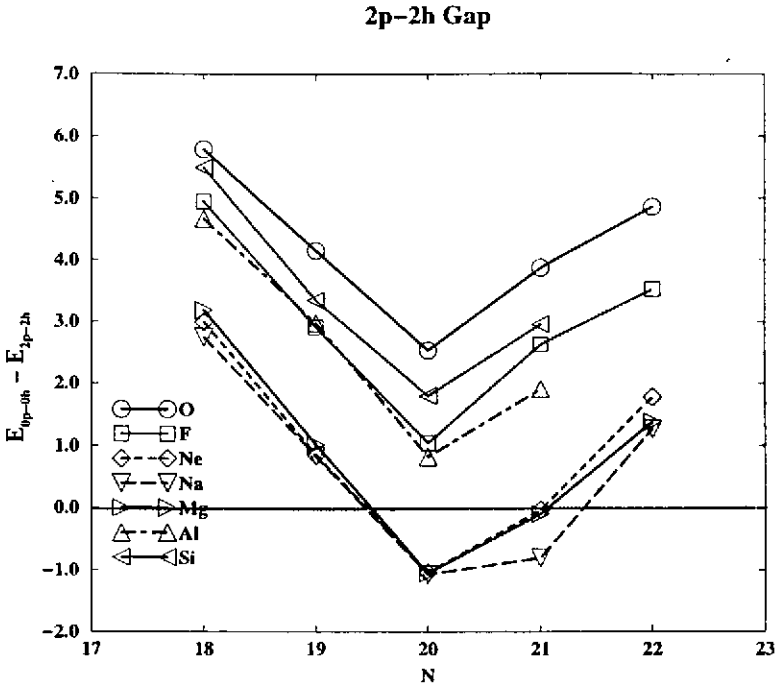

Figure 19: Energy of the 2p-2h intruders relative to the normally filled state

tive spherical mean field, that determines which are the "unperturbed" energies of the configurations that can maximize the correlations induced by the multipole hamiltonian, whose dominant terms, as we have seen in section 3, are pairing and quadrupole. Take ^{32}Mg; if we promote two neutrons to the pf-shell we open two new correlation channels; neutron-neutron pairing and proton-neutron quadrupole. This last one is particularly efficient because the orbits around the fermi level form Quasi-SU3 sequences.

In figure 19 we see the result of adding all these contributions. The intruder configurations are more bound in Ne, Na and Mg at N=20, for an amount that is roughly what is needed to restore the agreement with experiment in fig. 18. One can wonder, why not proton intruders? the reason is that the proton orbits are strongly bound due to the neutron excess, an extreme that we have verified explicitely. Another aspect is, why 2p-2h intruders and not 4p-4h intruders? Here we come back to the discussion of the balance between monopole and multipole. In short, in our calculation the extra gain of quadrupole energy in the 4p-4h intruder is not sufficient to compensate for the extra loss of monopole energy. It could be argued that this is interaction dependent, but we will show in a moment that the quadrupole properties strongly favour the 2p-2h intruder interpretation. If we mix properly the intruder and the normal configuration, the percentage of closed shell in the ground state is about 20% and we are entitled to speak of a shell closure that vanishes.

Lets focuss now on other known properties of ^{32}Mg, the excitation energy of the 2^+ and the BE2 of the $0^+ \rightarrow 2^+$ transition. The experimental values are ΔE=0.89 MeV [42] and BE2$\uparrow$=450 e^{2}fm^4 [49]. The theoretical results with N=20 closed are ΔE=1.71 MeV and BE2$\uparrow$=150 e^{2}fm^4. For the intruder state these values are ΔE=1.01 MeV and

BE2↑=500 e^2fm^4. The agreement is very good and if anything, we overshoot the BE2. This is normal because the mixing with the closed shell configuration will tend to reduce this number. This bring us to the question we had arisen on the role of 4p-4h intruders in ^{32}Mg. For that we compute the BE2↑ in this configuration and find 650 e^2fm^4 which is far bigger than the experimental number. Moreover, the jump in BE2 from the closed shell to the 2p-2h intruder is much larger than the jump from 2p-2h to 4p-4h. As the gain in quadrupole energy is roughly proportional to the BE2 value, the 4p-4h configurations are higher in energy than the 2p-2h ones. Therefore we conclude that the breaking of the N=20 shell closure is mainly the effect of 2p-2h intruders.

We can now proceed to see whether the intruders play a dominant role when neutrons are added or not. The answer is already seen in figure 19 where the intruders are not favoured energetically beyond N=21. The reason is that when we have particles in the pf-shell already in the normal filling, correlation channels that were not active at the closed shell are now open, therefore the relative correlation gain of the intruder is smaller, kind of what happened to the 4p-4h intruder at N=20. Thus the intruding region is limited to Z=10,11,12 and N=19,20,21, however we expect that at N=22 the "closed N=20" predictions will underestimate the collective properties.

We can extend our calculations until the neutron drip line is reached –actually we can overpass it without any problem beyond the conceptual one!–. We predict that ^{38}Mg is definitely bound while ^{40}Mg's $S_{2N} \sim 0$, precludes any conclusion. Notice here that the Relativistic mean field calculations of [53] place the drip line at a much lower value of N. All Mg isotopes from N=20 to N=28 are deformed and bear similar quadrupole moments (70-60 e fm^2) and B(E2)↑ (400-500 e^2fm^4). The excitation energy of the first 2^+ remains also very constant at around 1 MeV. The mean field calculations of [51] using Skyrme forces give results very close to ours for the deformation and for the location of the drip line. However they cannot explain the onset of deformation at N=20. This fact can be better understood in the mean field calculations of ref. [52] using the Gogny force. The energy *vs* deformation curves obtained with both forces are very similar. They present a spherical minimum and a shoulder at β=0.5. It is only when the Bohr hamiltonian is solved in the (β, γ) plane that a deformed ground state is obtained, and this calculation is only available for the Gogny force [52]. A more detailed comparison between the shell model and mean field results is in progress.

^{40}Mg represents a very special case in or results; it is the only N=28 isotone in which the neutron shell closure is clearly broken. We have plotted in figure 20 the 1f7/2 occupancies from Z=10 to Z=20. The effect of the Z=14 and Z=20 proton subshell closures in reinforcing the N=28 neutron closure is clearly seen. In ^{40}Mg we reach the minimum of the 1f7/2 shell ocupation, and, what is more important, the closed shell configuration has lost its leading status in the wave function because the configuration with two neutrons in the 2p3/2 orbit has an equivalent weigth (22% *vs* 28%). We must therefore admit that in our calculation N=28 is not a closed shell at Z=12.

7. CONCLUSIONS

The spherical shell model provides a description of the nuclear dynamics that makes it possible to keep a connexion with the basic initial ingredients of the problem, i.e. nucleons selfbound in vacuum by its mutual –non relativistic, two body– interaction. In the

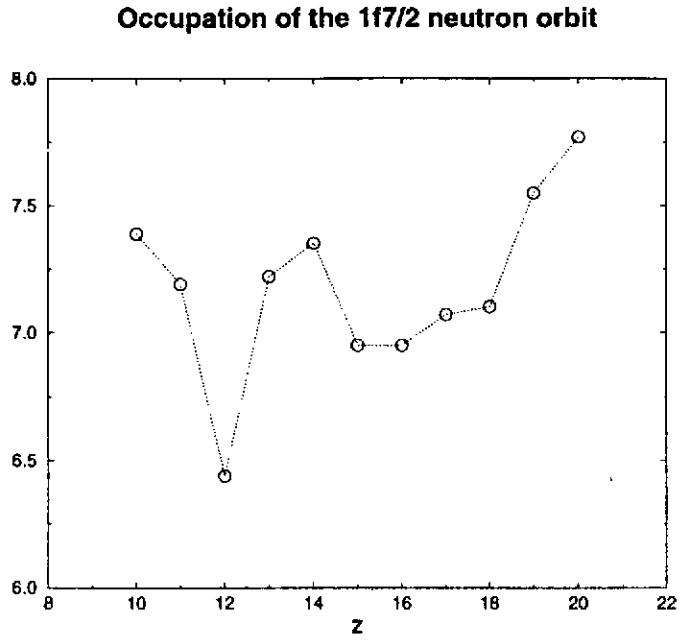

Figure 20: Occupation of the 1f7/2 orbit at N=28

route from the bare nucleon-nucleon to the prediction of the level scheme or decay properties of a particular nucleus, we have to pay many tolls; first, the bare interaction has to be regularized, and then, due to saturation problems, its monopole part fitted to the properties of the closed shells and closed shells +/− one nucleon. However, the separation of the effective interaction in monopole and multipole parts, and the realization that the multipole part of the realistic interactions is correct, paves the way to obtain an universal interaction for the shell model. Secondly, the valence spaces that contain the necessary degrees of freedom for a satisfactory description of the nuclear properties become exceedingly large for medium-heavy nucleus. Nevertheless, complete diagonalizations in the pf-shell, that have become recently available thanks to the impressive algorithmic advances of E. Caurier's codes, provide a realistic microcosmos in which many of the features of the heavier nuclei show up. In particular, collective deformed nuclei can be perfectly accounted for by the spherical shell model. Furthermore, sound indications on the symmetries or coupling schemes that will underlie the description of heavier nuclei are obtained, in the form of Elliott's SU3 variants. This approach has also proven to be able to encompass in the same framework the behaviour of nuclei far from stability, in spite of the increase of difficulty due to the lesser control that we have on the effective spherical mean field in very neutron (or proton) rich nuclei.

Acknowledgements I want to express my gratitude to the organizers of the Jolliot-Curie school for their warm hospitality, with an special mention to Prof. Yvon Abgrall. I want to thank E. Caurier, A. Zuker, J, Retamosa, F. Nowacki, G. Martinez-Pinedo, L. M. Robledo, J. L. Egido and S. Lenzi for their collaboration. This work was supported by DGICYT (Spain) grant PB93-263.

References

[1] J. P. Elliott, Proc. Royal Soc. London **A245**, 128 and 562 (1958).

[2] P. J. Brussaard and P. W. M. Glaudemans, "Shell Model Applications in Nuclear Spectroscopy" North Holland 1997.

K. Heyde, "The Nuclear Shell Model" Springer 1994.

J.B. French, in *International school of physics Enrico Fermi*, Course XXXVI, C. Bloch ed. (Academic Press, New York, 1966).

[3] B.A. Brown and B.H. Wildenthal, *Annu. Rev. Nucl. Part. Sci.* **38**, 29 (1988).

[4] A. P. Zuker in "Contemporary Nuclear Shell Models" Lecture Notes in Physics, vol 482, p. 93. X. W. Pan *et al.* eds. Springer 1997.

A. P. Zuker, in "Nuclear dynamics at short and long ranges", A. Gattone *et al.* eds. (World Scientific, Singapore) (To be published.)

[5] V. R. Pandharipande, I. Sick and P. K. A. deWitt Huberts, Rev. Mod. Phys. **69**, 981 (1997).

[6] A. P. Zuker, B. Buck and J. B. McGrory Phys. Rev. Lett. **21**, 39 (1968).

[7] S. Cohen and D. Kurath, Nucl. Phys. **73**, 1 (1965)

[8] B.H. Wildenthal *Prog. Part. Nucl. Phys.* **11** (1984) 5

[9] A. Abzouzi, E. Caurier et A. P. Zuker, Phys. Rev. Lett. **66**, 1134 (1991).

[10] M. Dufour et A.P. Zuker, Phys. Rev. C **54**, 1641 (1996).

[11] T. T. S. Kuo and G. E. Brown, Nucl. Phys. **A114**, 235 (1968).

[12] S. Kahana, H.C. Lee and C.K. Scott, Phys. Rev. **180**, 956 (1969); Phys. Rev. **185**, 1378 (1969).

[13] K.K. Mon and J.B. French, Ann. Phys. (NY) **95**, 90 (1975).

[14] J. B. French *et al* Adv. Nucl. Phys. **3**, 193 (1969)

[15] R. R. Whitehead *et al* Adv. Nucl. Phys. **9**, 123 (1977).

[16] R. R. Whitehead, in *Moment methods in many fermion systems*, edited by B. J. Dalton et al. (Plenum, New York, 1980).

[17] S. E. Koonin, D. J. Dean and K. Langanke, Phys. Reports **278**, 2 (1997).

[18] M. Honma, T. Mizusaki and T. Otsuka, Phys. Rev. Lett. **77**,3315 (1996)

[19] A. Poves and A. P. Zuker, Phys. Rep. **70**, 235 (1981).

[20] E. Caurier, A. P. Zuker, A. Poves, and G. Martínez-Pinedo, Phys. Rev. C **50**, 225 (1994).

[21] G. Martínez-Pinedo, A. P. Zuker, A. Poves and E. Caurier, Phys. Rev. C. **55**, 187 (1997).

[22] G. Martínez-Pinedo, A. Poves, E. Caurier and A. P. Zuker, Phys. Rev. C **53**, R2602 (1996).

[23] E. Caurier, G. Martínez-Pinedo, A. Poves and A. P. Zuker, Phys. Rev. C **52**, R1736 (1995).

[24] E. Caurier, A. Poves and A. P. Zuker, Phys. Rev. Lett. **74**, 1517 (1995).

[25] S. Lenzi *et al.*, Z. Phys. **A354**, 117 (1996).

[26] E. Caurier, J. L. Egido, G. Martínez-Pinedo, A. Poves, J. Retamosa, L. M. Robledo and A. P. Zuker, Phys. Rev. Lett. **75**, 2466 (1995).

[27] F. Brandolini **et al**, Heavy Ion Physics **5** (1997).

[28] A. Bohr and B. Mottelson, *Nuclear Structure* vol I (Benjamin, Reading, 1964).

[29] C. A. Ur *et al*, submitted to Phys. Rev. C

[30] G. Martínez-Pinedo, A. Poves, L. M. Robledo, E. Caurier, F. Nowacki, and A. P. Zuker, Phys. Rev. C **54**, R2150 (1996).

[31] S. Lenzi *et al* Phys. Rev. C **56**, 1313 (1997).

[32] A. Zuker, J. Retamosa, A. Poves and E. Caurier, Phys. Rev. C **52**, R1742 (1995).

[33] J. Retamosa, E. Caurier, F. Nowacki and A. Poves, Phys. Rev. C**55**, 1266 (1997).

[34] G. Audi and A. H. Wapstra, Nucl. Phys. **A565**, 1 (1993).

[35] T. R. Werner, J. A. Sheikh, W. Nazarewicz, M. R. Strayer, A. S. Umar and M. Misu, Phys. Lett. B**335** 259 (1994).

[36] H. Scheit *et al.*, Phys. Rev. Lett. **77**, 3967 (1996).

[37] T. Glasmacher *et al.*, Phys. Lett. **B395** 163 (1997)

[38] O. Sorlin *et al.*, Phys. Rev. C**47** 2941 (1993). O. Sorlin *et al.*, Nucl. Phys. **A583** 763 (1995).

[39] P. Baumann *et al*, Phys. Lett. **B228** 458 (1989)

[40] C. Thibault *et al.* Phys. Rev. C**12** 193 (1975).

[41] C. Detraz, D. Guillemaud, G. Huber, R. Klapisch, M. Langevin, F. Naulin, C. Thibault, L. C. Carraz and F. Touchard, Phys. Rev. C**19** 171 (1978).

[42] D. Guillemaud, C. Detraz, M. Langevin, F. Naulin, M. de Saint-Simon, C. Thibault, F. Touchard and M. Epherre, Nucl Phys A**246** 37 (1984).

[43] G. Klotz *et al*, Phys. Rev. **C47**, 2502 (1993).

[44] B. H. Wildenthal, M. S. Curtion and B. A. Brown, Phys. Rev. **C28**, 1343 (1983).

[45] X. Campi, H. Flocard, A. K. Kerman and S. Koonin, Nucl. Phys. A**251** 193 (1975).

[46] A. Poves and J. Retamosa, Phys. Lett B**184** 311 (1987). A. Poves and J. Retamosa, Nucl. Phys A**571** 221 (1994).

[47] E. K. Warburton, J. A. Becker and B. A. Brown, Phys. Rev. C**41** 1147 (1990).

[48] N. Fukunishi, T. Otsuka, and T. Sebe, Phys. Lett. **B296**, 1992 279.

[49] T. Motobayashi *et al*, Phys. Lett. **B346**, 9 (1995)

[50] E. Caurier, F. Nowacki, A. Poves and J. Retamosa, to be published.

[51] J. Terasaki, H. Flocard, P. H. Heenen and P. Bonche, Nucl. Phys. **A621**, 706 (1997).

[52] M. Girod and S. Peru, private communication.

[53] G. A. Lalazissis, D. Vretenar, W. Pöschl an P. Ring, nucl-th/9710013.